Biointerface Research in Applied Chemistry
Open-Access Journal (ISSN: 2069-5837)

Article
Volume 13, Issue 1, 2023, 65
https://doi.org/10.33263/BRIAC131.065

Simulation Study of Poly-Caprolactone, Chitosan, and Vinyl Ester Resin-coated Stainless Steel to Improve Corrosion Behavior, Bioactivity, and Biodegradability

Ersin Kamberli [1], Majid Monajjemi [1,2,*], Fatma Kandemirli [1], Fatemeh Mollaamin [1]

[1] Department of Biomedical Engineering, Faculty of Engineering and Architecture, Kastamonu University, Kastamonu, Turkey
[2] Department of Chemical engineering, Central Tehran Branch, Islamic Azad University, Tehran, Iran
* Correspondence: m_monajjemi@srbiau.ac.ir; maj.monajjemi@iauctb.ac.ir (M.M.);

Scopus Author ID 6701810683
Received: 22.11.2021; Accepted: 19.12.2021; Published: 2.02.2022

Abstract: Heterogeneous materials are usually found in industrial and chemical centers, such as metallic alloy, polymer blending, porous and cracked materials, and especially composites. We exhibited expanded detailed studies on the integration of bonding between poly-caprolactone (PCL), chitosan and vinyl ester resin (VER), and stainless steel (SS) with h-BN substrates. Using h-BN dielectrics leads us towards a suitable improvement in mobility relative and increasing surface activities. Furthermore, we exhibited that the integration of h-BN with stainless steel (SS) exhibits unique advantages compared to exfoliated graphene. We offered higher resistance and anti-corrosion for stainless steel by forming these polymer layers on the surface sheet. Therefore, biopolymer strongly can be suggested as a perfect antifouling coating solution owing to its broad-spectrum antibacterial, antifungal, and anti-algal properties, along with amazing film-forming properties. Although atomic coordinates are adjusted by this work to reduce the molecular energy, conformational changes in the polymers might be considered to obtain the macromolecules pair correlation function. Gyration rays and end-to-end distance distributions of the chains have been applied to measure polymers' flexibilities quantitatively.

Keywords: poly-caprolactone; chitosan; vinyl ester resin; coated stainless-steel; corrosion.

1. Introduction

Some metals can be used as implants for biomedical usage because of their suitable properties [1, 2]. Most of them are used *in vivo* due to high stability as well as low degradation rate [3, 4]. But sometimes, they lead to some difficulties such as the failure to stimulate the tissue growing, release of metal ions into the environment, and inflammation in the body [4, 5]. Since metal implants are heavy [6–8], technology has been progressed towards using lightweight materials to tissue in growth. Stainless steels (such as 316L SS) are usually used for biomedical materials—including in joint replacements, stents, and orthopedics—due to their offering of unique advantages in wonderful corrosion resistance [9–11]. These metal ions are too toxic and have potential health hazards that cause bad allergies and probably cancer tumors [12, 13]. One of the problems is that the corrosion resistance of 316L SS can be improved via coating with various protective films [14–21]. Huang *et al*. [16] reported that coating 316L SS with superhydrophobic TiO_2 nanotube arrays could decrease platelet adhesion

and increase corrosion resistance. Wang *et al*. [18] exhibited that a 316L SS surface modified with zirconium compounds makes the blood compatibility and corrosion resistance in high quality. Stainless steel within poly-caprolactone/chitosan-coated has recently attracted the attention of many scientists due to its high strength-to-weight ratio and degradability. In addition, the stress shielding phenomenon does not occur for stainless steel (SS) alloys due to having density and Young's modulus close to that of natural bone. Chitosan (Figure 1) is a polysaccharide composed of randomly distributed β-(1→4)-linked D- glucosamine and *N*-acetyl-D- glucosamine. As an industrial material, it can also be used in a self-healing polyurethane paint coating.

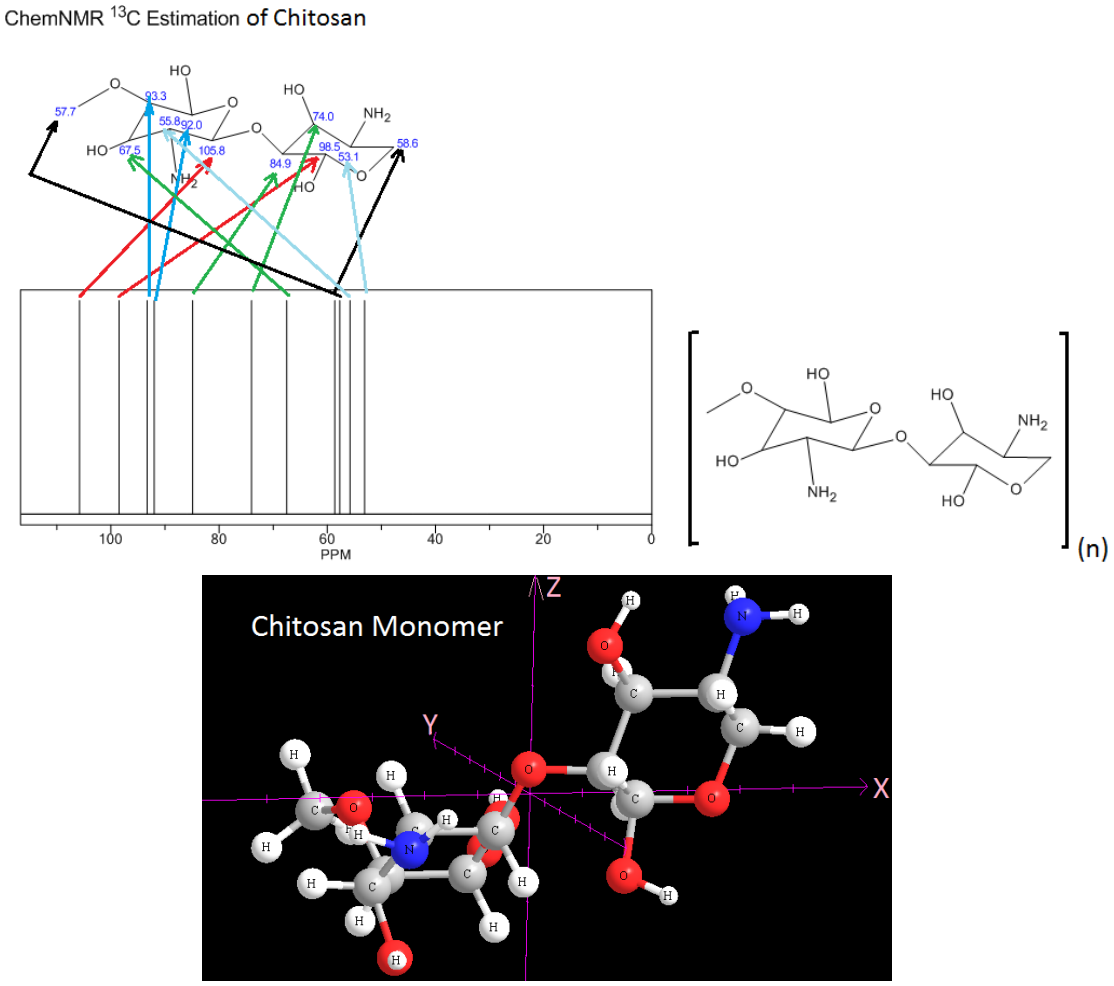

Figure 1. A monomer of optimized chitosan structure and its NMR orientation.

In medicine, it is useful to help deliver drugs via the skin. Moreover, chitosan is part of a green chemistry project, mainly extracted from marine shellfish wastes (Scheme 1). The amine groups are also responsible for the low hydrophobicity of chitosan in an acidic medium [22-25]. The cross-linking of chitosan molecules via the reaction of primary amine groups in chitosan with aldehyde groups from the cross-linker glutaraldehyde (GA) increases tensile strength hydrophobicity and enhanced chemical resistance. Apart from the newly formed imine group, a number of amine groups remain in the cross-linked chitosan, allowing interaction with the surroundings [24, 25]. Poly-caprolactone (PCL) is a biopolymer with wide capabilities and unique character as an important biomaterial compound for bone tissue biomedical engineering, cartilage repair, wound dressing, and cardiovascular tissue engineering [26–29]. PCL is one of the most commercially available synthetic polymers characterized by huge biodegradation, including special mechanical behaviors that could be generally controlled via

regulating the local environmental driving interactions. This polymer is usually used as an additive in various resins for improving their processing behaviors, such as impact resistance. PCL also can be mixed with starch to lower its cost and increase biodegradability, or it can be added as a polymeric plasticizer to polyvinyl chloride (PVC) [30]. Poly-caprolactone is also used for a splinter, splinting, modeling, and feedstock for prototyping systems such as fused filament three-dimensional printers. It can be synthesized using a suitable catalyst with a ring-opening polymerization phenomenon (Figure 2).

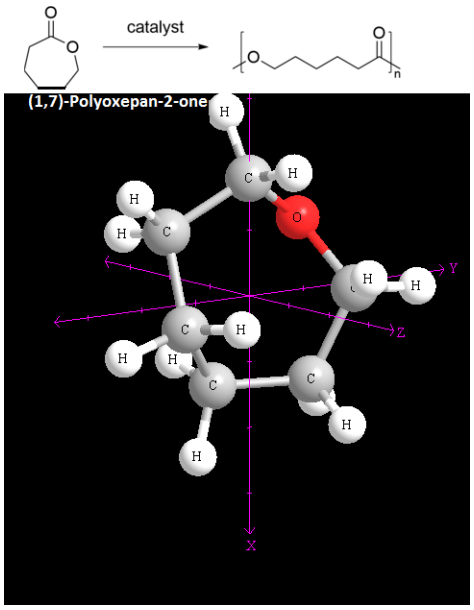

Figure 2. Optimized poly-caprolactone (PCL) as an important biopolymer.

PCL has mechanical properties of a suitable tough, analogous to nylon and plastic, which softens at around 62°C, then becomes similar a putty-like consistency and is quickly shaped through immersing in warm water. PCL has low conductivity; therefore, it is easy to make a structure by hand at this temperature. This makes it perfect for preparing small-scale modeling instruments and repairing plastic objects. Although softened PCL readily sticks to several other plastics at a higher temperature, the stickiness can be minimized if the surface is cooled while still leaving the mass pliable. By this work, we have shown a system by mixing poly-caprolactone/chitosan can be coated with a wide range of metals against any corrosions. This mixture layer (one layer after another) affects the strength and durability of metal and makes the materials inexpensive. This kind of coating prevents equipment damage and product leakage, especially crucial in chemical industries, thereby saving and caring for the environment. The performance and lifetime of metals or any other substrate can be increased by applying a suitable anti-corrosion coating, especially layer by layer coating (poly layer coating or PLC). PLC makes several barrier dams over the metal surface against corrosion attack. For accomplishing an excellent PLC it is needed to consider several items of corrosion, including (1) providing a galvanic situation for the anti-corrosion by using different electrochemical charges, for instance "Inter-granular Corrosion" which is a kind of corrosion that occurs when the grain boundaries in a metal form an anode and the interior of the grain act as a cathode, (2) "Stress-corrosion Cracking (SCC)", that is a result of stress due to cold work, thermal process or welding. (3) "Crevice Corrosion" which is due to the attack of metal surfaces in crevices, such as edges of rivet heads and nuts (Scheme 1).

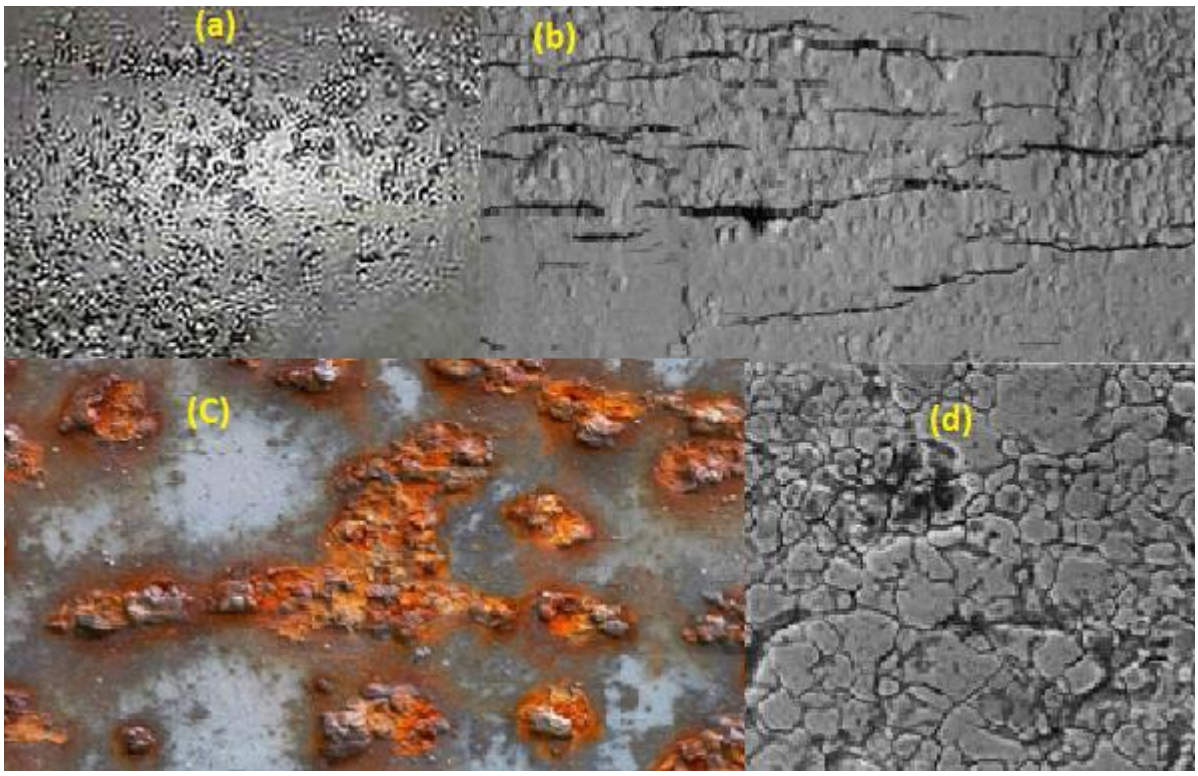

Scheme 1. (**a**, **c**) Pitting corrosion; (**b**) stress-corrosion cracking (SCC); (**d**) Inter-granular corrosion.

Corrosive substances like dust or sand accumulate on the surface and create an environment for water to get collected and corrode the material (4) "Pitting Corrosion", a localized form of corrosion leading to small holes or pits on a metal surface. Its mechanism works in the same manner as in crevice corrosion. For removing these problems, we used a mixture of polymers, including poly-caprolactone/chitosan/vinyl ester resin.

VER can be replaced as an alternative to polyester materials due to polyester and epoxy groups (Figure 3). Vinyl-ester has low viscosity, high resistance in corrosion, physical adhesion compared to polyester because of polar hydroxyl and ether groups. Vinyl ester resins are obtained by adding epoxy resins with unsaturated carboxylic acid monomers. The unique physical and chemical properties of "VER" have attracted much interest for marine industrial applications.

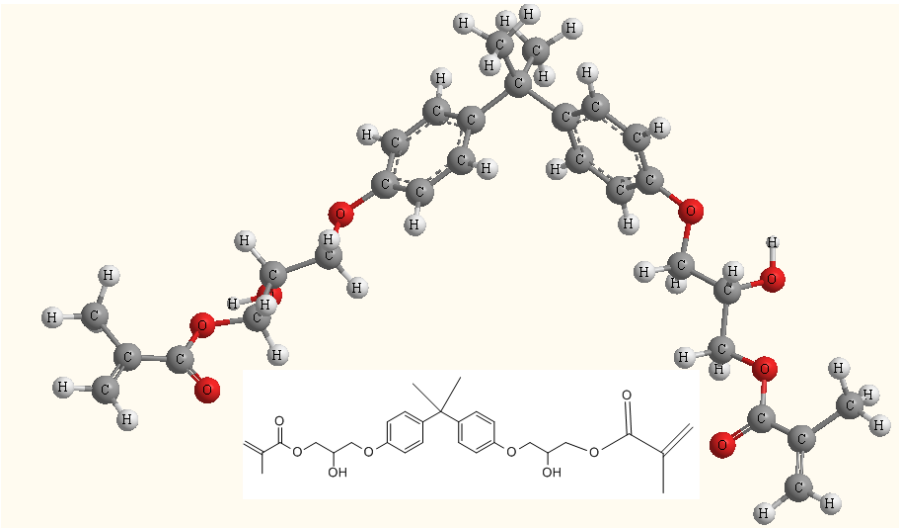

Figure 3. Geometry optimization "vinyl ester" via ab-initio calculation.

VE resin exhibits suitable mechanical properties, same as epoxy, and offers process abilities, same as a polyester resin. VER is a major material for manufacturing several thermosets widely applied in industrial goods. By this work, the mechanical properties of SS/h-BN in the presence of poly-caprolactone/chitosan/vinyl ester resin have been investigated through computational modeling and simulation approaches. It is notable that any testing of the nanocomposite properties completely depends on the microstructure situation and the fabrication process of those materials. Any exfoliation to optimize filler orientation might be hard to reach, and the VE chain preferably extends among h-BN particles.

2. Materials and Methods

2.1. Description of simulation.

A simulation of steel alternating with a composite made of poly-caprolactone/chitosan/vinyl ester resin reinforced with h-BN sheets using Molecular Dynamics (MD) has been accomplished. The effect of the polymer's chains length and the adhesion energies are modeled by several situations. Designing suitable interphase between the metal and those polymer layers is the main target of our simulation to find the best position of mechanical properties. We have focused on polymer-to-metal substrate interactions linked to interfacial non-bonded interaction (van der Waals and electrostatic potentials) between the atoms of the polymer and the atoms in the metal oxide on the surface. Scheme 2 shows a vinyl ester to steel bond. It is extremely difficult to perform measurements of stress and strain in the interphase through experimental testing due to in- accessibility to any kind of sensor (Figure 4). Cohesive densities of energies, polymers packaging, or localized situation in the macromolecule chains can be determined by molecular modeling techniques.

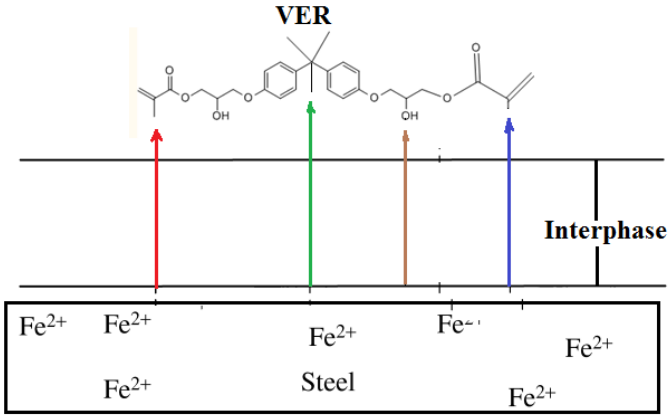

Scheme 2. Vinyl ester to steel bond.

2.2. Simulation Methodology and analyzing.

MD simulations were done in an isothermal-isobaric (NPT) statistical ensemble, using the Charm package [31]. Several pressure using Berendsen barostat was kept constant at P = 1 up to 2 atm. The stochastic velocities were used to maintain the temperature among T =300-400 K. The integration time steps were selected between 0.2-0.4 fs, and periodic boundary conditions have been applied in all three dimensions. Finally, the best simulation occurred in P=1atm, time steps=0.5, and T=300 K. To obtain initial PCL/SS/h-BN or VERL/SS/h-BN layers were placed at a close distance. In data analysis, we exclude a certain number of configurations, such as our results independent of the initial state. Non-bonded interactions

among PCL/SS/Chitosan atoms (Figure 1) with carbon, iron, and nitrogen of PCL/SS/h-BN complexes, including $\sigma_i - \sigma_j$ interaction, C-$metal$ interaction, Fe-σ_i , OH, H-bonds are shown in (Figure 4).

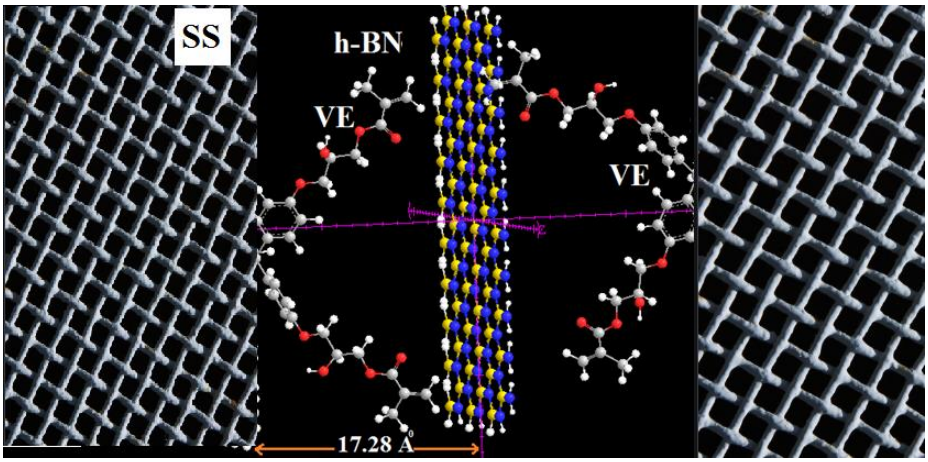

Figure 4. A simulation of steel alternating with a composite made of SS /Vinyl ester resin reinforced with h-BN sheets.

Table1. Non-bonded parameters in terms of E $_{(van\ der\ waals)}$ + E $_{(Coulomb)}$.

Non bonded interaction

$$V_{LJ}(r_{ij}) = 4\varepsilon_{ij}\{[\left(\frac{\sigma_{ij}}{r_{ij}}\right)^{12} - \left(\frac{\sigma_{ij}}{r_{ij}}\right)^{6}]\}, r < R_C$$

Atom type	**Mass(g/mol)**	$\boldsymbol{\sigma(nm)}$	$\boldsymbol{\varepsilon(\frac{kcal}{mol})}$
CH_2	14.50	0.355	0.0.08
C=O	28.35	0.415	0.115
O-H	17.18	0.212	0.015
C-O	28.55	0.425	0.112
C-C	24.15	0.134	0.060
Fe(SS)	56.70	0.333	0.090
CH_3	15.55	0.315	0.056
h-BN	19.03	0.45	0.88

Table 2. Parameters of bonded interactions of the atomistic force field.

Bonded & angle interaction

$$\{[V_b(r_{ij}) = \sum_{bonds} k_{ij}^{b}\,(r_{ij} - b_{ij})^2]\} + \{[V_\beta(\theta_{ijk}) = 0.5 \sum_{angle} k_{ijk}^{\theta}(\theta_{ijk} - \theta_{ijk}^{0})^2]\} + \{[V(\varphi_{ijkl})\, k_\varphi(1 + Cos(n\varphi - \delta)$$

bond	b(Å)	k^b kcal/mol* Å^2	angle	θ_{ijk}^0	k_{ijk}^{θ} $(\frac{\text{kcal}}{mol} * Rad^2)$	Dihedral φ_{ijkl}	k_φ kcal/mol	n	δ
CH2	1.10	335	C-O-C	116.5	53.5	C-C-C-O	0.35	1	0.00
C=O	1.25	345	C-C-C	123.5	60.1	H-C-C-C	0.40	3	180.0
O-H	1.12	365	O-C-O	120.5	42.5	O-C-C-H	0.20	2	0.00
C-O	1.30	235	C-C-H	115.5	42.1	C-O-C-H	0.55	2	0.00
C-C	1.35	445	H-C-H	110.5	61.5	H-C-C-H	0.35	1	180.0
Fe(SS)	1.25	355	O-C-H	120.5	42.5	O-C-C-O	0.65	3	90.0
CH3	1.35	235	C-C-C	120.5	55.5	C-C-C-C	0.20	1	0.00
h-BN	1.15	335	B-N-B	115.5	41.5	B-N-B-N	0.20	1	180.0

* For Fe (SS) & h-BN sheets the formula of $(V_\beta(\theta_{ijk}) = 0.5 \sum_{angle} k_{ijk}^{\theta}(Cos\theta_{ijk} - Cos\theta_{ijk}^{0})^2]\}$ has been used

Using Molecular Dynamics (MD), these interactions are explained via spherically truncated Lennard–Jones potentials as follows: $V_{LJ}(r_{ij}) = 4\varepsilon_{ij}\{[\left(\frac{\sigma_{ij}}{r_{ij}}\right)^{12} - \left(\frac{\sigma_{ij}}{r_{ij}}\right)^{6}]\}, r < R_C$ **(1),** $R_C$is a cutoff distance around 12 Å for VE. In addition, the Lorentz–Berthelot rules via

arithmetic middle have been applied for the interactions among VE and h-BN atoms as follows "$\sigma_{ij} = 0.5(\sigma_i + \sigma_j)"and\ \varepsilon_{ij} = \sqrt{\varepsilon_i} * \sqrt{\varepsilon_j}$. **(2)**. the non-bonded and bonded parameters, including van der Waals of related force fields, are listed in Tables 1 and 2 for both VER and h-BN [32-34]. The total energy of the model system is a total of several partial energies as follows: $E_{(system)} = E_{(bond)} + E_{(angle)} + E_{(torsion)} + E_{(over)} + E_{(vdW)} + E_{(Coulomb)} + E_{(Specific)}$, **(3),** where $E_{(bond)}$ is the energy associated with the bond formation and ($E_{(angle)} + E_{(torsion)}$) are the energies associated with valence angle strain and torsional angle strain, respectively $E_{(over)}$ energies associated with valence angle strain and torsional angle strain, respectively, is an energy penalty term that prevents the over-coordination of the atoms. $E_{vdW} + E_{(Coulomb)}$ are the dispersive, electrostatic energy contribution between all atoms; respectively, and $E_{(Specific)}$ is a system-specific energy term that may include lone-pair, conjugation, hydrogen bonding.

3. Results and Discussion

3.1. Modelling of poly-caprolactone/chitosan/vinyl ester resin.

Nine polymers, including poly-caprolactone/chitosan/vinyl ester resin reinforced with h-BN sheets, have been modeled with MD simulation. They differ in the structures and different lengths of their chains for each configuration [35]. Their lengths can be estimated via the distribution of inter entanglement strands in real polymers. It is possible to define a linkage between the atomistic simulation and the mesoscale polymers modeling. The statistical length (b) is based on mean squared end-to-end distance accordance with the model$b = \frac{<R^2>}{L}$ (4). The molar mass can be calculated via multiplying the Kuhn length by the unit length of the real chain, and consequently, it is possible to obtain the packing length and the ratio of the volume. So by this model, it is possible to simulate thousands of atoms for a suitable molecular dynamics calculation. Figure 5 exhibits a polymer chain with three vinyl ester monomers using the CPK-Dreiding model.

Table 3. Parameters of the four different polymers models by the MD simulation.

Macromolecules	C(Å)	Number of chains	Number of configurations
Poly-caprolactone			
Polymer 1	14.3	16	3
Polymer 2	15.5	17	3
Polymer 3	15.9	18	3
Vinyl ester resin			
Polymer 1	16.3	12	3
Polymer 2	16.6	13	3
Polymer 3	17.2	15	3
Chitosan			
Polymer 1	12.5	16	3
Polymer 2	13.3	14	3
Polymer 3	12.9	17	3

PBCs or Periodic boundary conditions have to be generated in all directions, consisting of pressure, volume, and temperature positions are prepared constantly. A rectangular prism with edge lengths a = 27.1 Å and b = 28.9 Å was selected to build the unit cell. Table 3 exhibits the structural parameters of the 3 different model polymers of each poly-caprolactone/chitosan/vinyl ester resin used in the MD simulation.

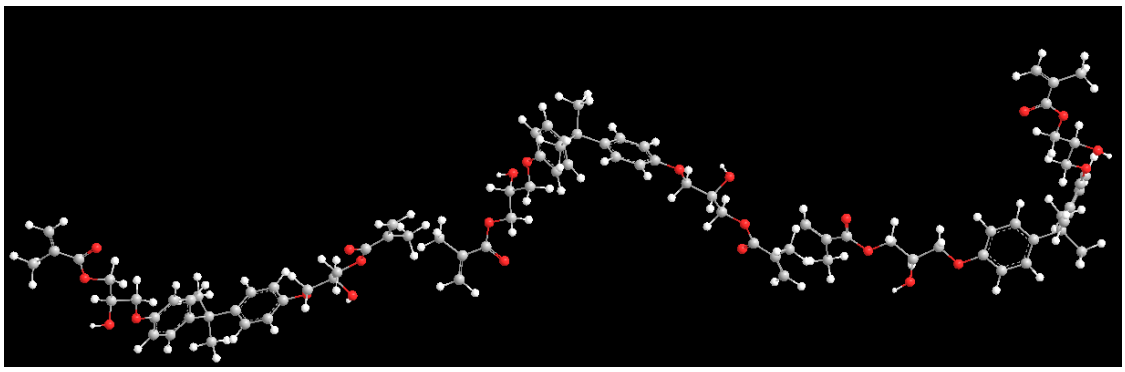

Figure 5. Representation of a polymer chain with three vinyl ester monomers.

Based on work in reference [36], the polymers optimized based on the following procedure of atomic force cutoff of 0.2 (kcal/mol) up to a maximum of 1000 iteration steps, using the Fletcher–Reeves algorithm [37]. This method works have been done based on our previous works [38-55] and some novel works in two past years [56-84].

3.2. Modeling of the metal surface.

We model a single cell of ferrous oxide and cleave the (111) plane to obtain the interface forces among the oxide and several polymers. The metal structure is relaxed and held rigid during the simulation (Except the polymer chains that permit to move). The force field used in the MD calculation is OPLS & COMPASS. Although the surface is ionic, the OPLS & COMPASS force fields require bonds between the iron and oxygen atoms. A supercell is built with lattice parameters a = 25.9 Å, b = 29.1 Å and c = 12.9 Å, for suitable fitting. Only the polymer atoms close to the interface move to approach the metal substrate due to the non-bonding interactions at the surface. This procedure has been followed for the four different polymers used. Figure 6 shows the box with iron (II) oxide and polymer layers.

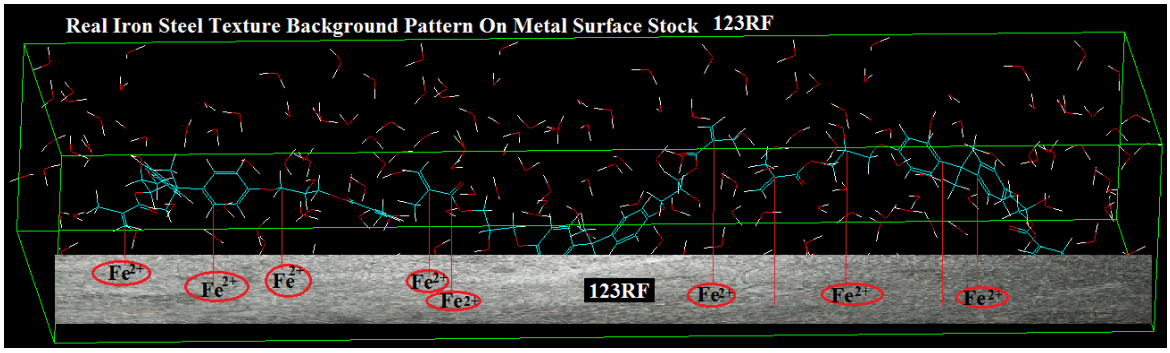

Figure 6. Interaction of on the surface of 123RF SS with polymer chain with three vinyl ester monomers.

Interaction between polymers and SS surface at the interface is modeled via 20 ps of NVT at 298-300 K. Time step of 0.5 fs has been applied for 10000 steps. Figure 7 exhibits the fluctuations of 10 K close to the equilibrium temperature, and the energies of various interactions have been calculated via the following formula.

Table 3 exhibits interaction energies between poly-caprolactone/chitosan/vinyl ester and SS/iron (II) oxide for the three models of each polymer, as calculated using MD, using equation (5). In order to quantify the capacity of molecules to adopt a more compact conformation, the radius of gyration (S^2) in each polymer before and after the application of MD has been calculated from the equation as follows, $S^2 = \frac{\sum_{i=1}^{N} m_i S_i^2}{\sum_{i=1}^{N} m_i}$ (6), where m_i is the

atomic weight. Figure 8 exhibits the radii of gyration for three polymers of increasing chain length. The longer chains have larger changes in their gyration during the macromolecule interacts with the SS-Fe^{2+} sheet. The pair correlation function of each poly-caprolactone/chitosan/vinyl ester macromolecules has been derived before and after the polymers interacted with the SS/iron (II) oxide.

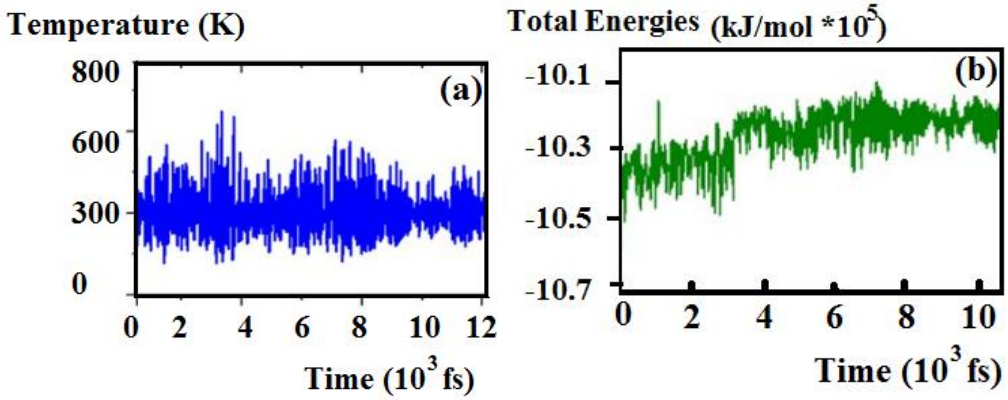

Figure 7. Fluctuations close to the equilibrium temperature and the energies for SS/VER interaction.

$E_{interaction} = E_{total} - (E_{surface} + E_{polymer})$ (5) Where: E_{total} is the whole energy of the system in the equilibrium position, $E_{surface}$ is the energy of oxide surface before the interaction, and $E_{polymer}$ is the energy of the bulk polymer. The $E_{interaction}$ of SS-polymers for poly-caprolactone/chitosan/vinyl ester resin reinforced with h-BN sheets are listed in Table 4.

Table 4. Interaction energies between poly-caprolactone/chitosan/vinyl ester and SS/iron (II) oxide.

Macromolecules	Total energies (kJ/mol 10^5)	Surface energies (kJ/mol 10^5)	Polymers energies (kJ/mol)	Interaction energies (kJ/mol)
Poly-caprolactone				
Polymer 1	-10.93773	-10.97565	4356	-564
Polymer 2	-10.94476	-10.97565	3542	-453
Polymer 3	-10.96243	-10.97565	1987	-665
Vinyl ester resin				
Polymer 1	-10.53815	-10.55463	2323	-675
Polymer 2	-10.52796	-10.55463	3423	-756
Polymer 3	-10.53052	-10.55463	3287	-876
Chitosan				
Polymer 1	-10.60462	-10.65465	5456	-453
Polymer 2	-10.62694	-10.65465	3425	-654
Polymer 3	-10.63170	-10.65465	2879	-584

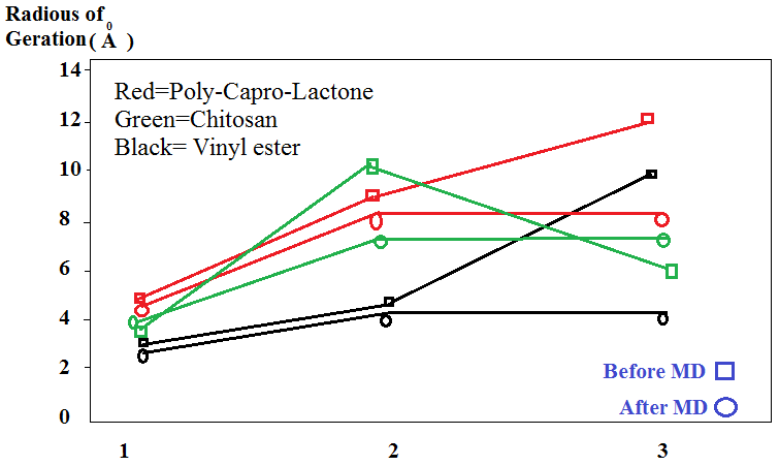

Figure 8. Radii of gyration for macromolecules of increasing chain length.

End-to-end length is another variable for estimating the potential of the macromolecules to change the configuration of polymers as the interaction with the SS-Fe^{2+} sheet proceeds (Fig.7). After the interaction of the poly-caprolactone/chitosan/vinyl ester with the SS-Fe^{2+}sheet, the probability of finding more folded chains increases, as predicted by MD calculations. At the same time, the accumulated probability of occurrence of unfolded chains decreases after the interaction is established. In these systems, more atoms of poly-caprolactone/chitosan/vinyl ester get closer to the SS-Fe^{2+} sheet and contribute collectively to increasing the interaction (adhesion) energy of the system.

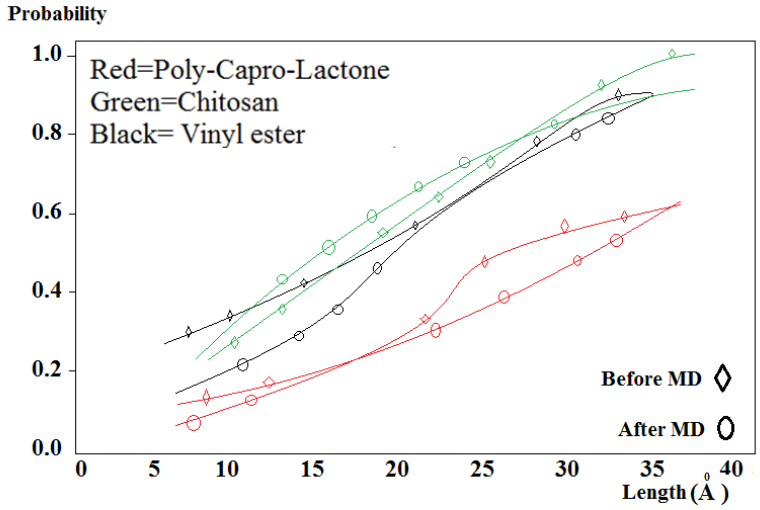

Figure 9. Interaction of the poly-caprolactone/chitosan/vinyl ester with the metallic substrate, as predicted by MD calculations (Polymer 3).

4. Conclusions

The computational prediction of physical properties in poly-caprolactone/ chitosan/ vinyl ester -to- SS-Fe^{2+} sheet interactions is especially challenging. MD simulation of the adhesion phenomena in the poly-caprolactone/chitosan/vinyl ester to SS-Fe^{2+} sheet bond has derived from MD simulation and applied as a means to study changes in the chains flexibilities as the length increases: end-to-end distance and consequently radius of gyration. This increases the non-bonded interaction between poly-caprolactone/chitosan/vinyl ester and SS-Fe^{2+}sheet atoms, as it is reflected in the amounts of the calculated energies of adhesion. Our results exhibit that End-to-end distances of the chains vary as the polymers interact with the metal surface with the sequence poly-caprolactone>chitosan>vinyl ester: the polymer chains fold out to adapt themselves to the SS-Fe^{2+} sheet. The radius of gyration in the poly-caprolactone > chitosan> vinyl ester chains increase as the number of monomers increases. SS-Fe^{2+} sheet with these coated polymers effectively will increase the amount biocompatible of materials. The potential coted of SS-Fe^{2+} sheet is useful for the surface modification of implants used in human bodies.

Funding

This study was supported by Kastamonu University Scientific Research Coordination Unit. Project Number KÜ-BAP01/2021-44.

Acknowledgments

We thank the Kastamonu University Scientific Research Studies Project Management Coordination. The authors are also grateful to Kastamonou University Central Research Laboratory Application and Research Center.

Conflicts of Interest

The authors declare no conflict of interest.

References

1. Saini, M.; Singh, Y.; Arora, P.; Arora, V.; Jain, K. Implant biomaterials: A comprehensive review. *World J. Clin.Cases* **2015**, *3*, 52-57, https://dx.doi.org/10.12998%2Fwjcc.v3.i1.52.
2. Katti, K.S. Biomaterials in total joint replacement. *Colloids Surf. B Biointerfaces* **2004**, *39*, 133-142, https://doi.org/10.1016/j.colsurfb.2003.12.002.
3. Oldani, C.; Dominguez, A. Titanium as a Biomaterial for Implants. *In: Recent Adv. Arthroplast. Fokter, S (Ed.)*, IntechOpen, London, UK **2012**, https://doi.org/10.5772/27413.
4. Sing, S.L.; Yeong, W.Y.; Wiria, F.E. Selective laser melting of titanium alloy with 50 wt % tantalum: Microstructure and mechanical properties. *J. Alloy. Compd.* **2016**, *660*, 461-470, https://doi.org/10.1016/j.jallcom.2015.11.141.
5. Zhao, X.; Niinomi, M.; Nakai, M.; Hieda, J. Beta type Ti-Mo alloys with changeable Young's modulus for spinal fixation applications. *Acta Biomater.* **2012**, *8*, 1990-1997, https://doi.org/10.1016/j.actbio.2012.02.004.
6. Niinomi, M.; Nakai, M.; Hieda, J. Development of new metallic alloys for biomedical applications. *Acta Biomater.* **2012**, *8*, 3888-3903, https://doi.org/10.1016/j.actbio.2012.06.037.
7. Mani, G.; Feldman, M.D.; Patel, D.; Agrawal, C.M. Coronary stents: A materials perspective. *Biomaterials* **2007**, *28*, 1689-1710, https://doi.org/10.1016/j.biomaterials.2006.11.042.
8. Karimi, S.; Nickchi, T.; Alfantazi, A.M. Long-term corrosion investigation of AISI 316L, Co-28Cr-6Mo, and Ti-6Al-4V alloys in simulated body solutions. *Appl. Surf. Sci.* **2012**, *258*, 6087-6096, https://doi.org/10.1016/j.apsusc.2012.03.008.
9. Williams, R.L.; Brown, S.A.; Merritt, K. Electrochemical studies on the influence of proteins on the corrosion of implant alloys. *Biomaterials* **1988**, *9*, 181-186, https://doi.org/10.1016/0142-9612(88)90119-6.
10. Tang, Y.C.; Katsuma, S.; Fujimoto, S.; Hiromoto, S. Electrochemical study of Type 304 and 316L stainless steels in simulated body fluids and cell cultures. *Acta Biomater.* **2006**, *2*, 709-715, https://doi.org/10.1016/j.actbio.2006.06.003.
11. Okazaki, Y.; Gotoh, E. Metal release from stainless steel, Co–Cr–Mo–Ni–Fe and Ni–Ti alloys in vascular implants. *Corros. Sci.* **2008**, *50*, 3429-3438, https://doi.org/10.1016/j.corsci.2008.09.002.
12. Takahashi, H.; Kinbara, M.; Sato, N.; Sasaki, K.; Sugawara, S.; Endo, Y. Nickel allergy-promoting effects of microbial or inflammatory substances at the sensitization step in mice. *Int. Immunopharmacol.* **2011**, *11*, 1534-1540, http://dx.doi.org/10.1016/j.intimp.2011.05.010.
13. D'Antò, V.; Eckhardt, A.; Hiller, K.A.; Spagnuolo, G.; Valletta, R.; Ambrosio, L.; Schmalz, G.; Schweikl, H. The influence of Ni(II) on surface antigen expression in murine macrophages. *Biomaterials* **2009**, *30*, 1492-1501, https://doi.org/10.1016/j.biomaterials.2008.12.004.
14. Li, J.; Zhang, X.; He, X.; Hang, R.; Huang, X.; Tang, B. Preparation, biocompatibility and wear resistance of microstructured Zr and ZrO_2 alloyed layers on 316L stainless steel. *Mater. Lett.* **2017**, *203*, 24-27, https://doi.org/10.1016/j.matlet.2017.05.106.
15. Al-Rashidy, Z.M.; Farag, M.M.; Abdel Ghany, N.A.; Ibrahim, A.M.; Abdel-Fattah, W.I. Aqueous electrophoretic deposition and corrosion protection of borate glass coatings on 316L stainless steel for hard tissue fixation. *Surf. Interfaces* **2017**, *7*, 125-133, https://doi.org/10.1016/j.surfin.2017.03.010.
16. Huang, Q.; Yang, Y.; Hu, R.; Lin, C.; Sun, L.; Vogler, E.A. Reduced platelet adhesion and improved corrosion resistance of superhydrophobic TiO_2-nanotube-coated 316L stainless steel. *Colloids Surf. B: Biointerfaces* **2015**, *125*, 134-141, https://doi.org/10.1016/j.colsurfb.2014.11.028.

17. Sharifnabi, A.; Fathi, M.H.; Eftekhari Yekta, B.; Hossainalipour, M. The structural and bio-corrosion barrier performance of Mg-substituted fluorapatite coating on 316L stainless steel human body implant. *Appl. Surf. Sci.* **2014**, *288*, 331-340, https://doi.org/10.1016/j.apsusc.2013.10.029.
18. Wang, L.; Zhao, X.; Ding, M.H.; Zheng, H.; Zhang, H.S.; Zhang, B.; Li, X.Q.; Wu, G.Y. Surface modification of biomedical AISI 316L stainless steel with zirconium carbonitride coatings. *Appl. Surf. Sci.* **2015**, *340*, 113-119, https://doi.org/10.1016/j.apsusc.2015.02.191.
19. Chang, S.H.; Chen, J.Z.; Hsiao, S.H.; Lin, G.W. Nanohardness, corrosion and protein adsorption properties of $CuAlO_2$ films deposited on 316L stainless steel for biomedical applications. *Appl. Surf. Sci.* **2014**, *289*, 455-461, https://doi.org/10.1016/j.apsusc.2013.11.004.
20. Cheng, I.C.; Chang, S.H.; Lin, G.W.; Chi, C.T.; Hsiao, S.H.; Chen, J.Z. Effect of Al/Cu ratios on the optical, electrical, and electrochemical properties of Cu-Al-Ca-O thin films. *J. Alloy. Compd.* **2014**, *609*, 111-115, https://doi.org/10.1016/j.jallcom.2014.04.146.
21. Chang, S.H.; Liou, J.S.; Huang, B.Y.; Chan, W.J.; Tsao, Y.T. Surface characteristics of the 316L stainless steel modified by ethylene vinyl acetate/chitosan composite films. *Surf. Coat. Technol.* **2017**, *320*, 635-639, https://doi.org/10.1016/j.surfcoat.2016.10.031.
22. Sadeghzade, S.; Emadi, R.; Tavangarian, F.; Naderi, M. Fabrication and evaluation of silica-based ceramic scaffolds for hard tissue engineering applications. *Mater. Sci. Eng.: C* **2017**, *71*, 431-438, https://doi.org/10.1016/j.msec.2016.10.042.
23. Kumar, S.; Ye, F.; Dobretsov, S.; Dutta, J. Chitosan nanocomposite coatings for food, paints, and water treatment applications. *Appl. Sci.* **2019**, *9*, 2409, https://doi.org/10.3390/app9122409.
24. Kong, M.; Chen, X.G.; Xing, K.; Park, H.J. Antimicrobial properties of chitosan and mode of action: A state of the art review. *Int. J. Food Microbiol.* **2010**, *144*, 51-63, https://doi.org/10.1016/j.ijfoodmicro.2010.09.012.
25. Kumar, S.; Mudai, A.; Roy, B.; Basumatary, I.B.; Mukherjee, A.; Dutta, J. Biodegradable hybrid nanocomposite of chitosan/gelatin and green synthesized zinc oxide nanoparticles for food packaging. *Foods* **2020**, *9*, 1143, https://doi.org/10.3390/foods9091143.
26. Nair, L.S.; Laurencin, C.T. Biodegradable polymers as biomaterials. *Prog. Polym. Sci.* **2007**, *32*, 762-798, https://doi.org/10.1016/j.progpolymsci.2007.05.017.
27. Mondal, D.; Griffith, M.; Venkatraman, S.S. Polycaprolactone-based biomaterials for tissue engineering and drug delivery: Current scenario and challenges. *Int. J. Polym. Mater. Polym. Biomater.* **2016**, *65*, 255-265, https://doi.org/10.1080/00914037.2015.1103241.
28. Okada, M. Chemical syntheses of biodegradable polymers. *Prog. Polym. Sci.* **2002**, *27*, 87-133, https://doi.org/10.1016/S0079-6700(01)00039-9.
29. Williams, J.M.; Adewunmi, A.; Schek, R.M.; Flanagan, C.L.; Krebsbach, P.H.; Feinberg, S.E.; Hollister, S.J.; Das, S. Bone tissue engineering using polycaprolactone scaffolds fabricated via selective laser sintering. *Biomaterials* **2005**, *26*, 4817-4827, https://doi.org/10.1016/j.biomaterials.2004.11.057.
30. Neto, C.G.T.; Giacometti, J.A.; Job, A.E.; Ferreira, F.C.; Fonseca, J.L.C.; Pereira, M.R. Thermal analysis of chitosan based networks. *Carbohyd. Polym.* **2005**, *62*, 97-103, https://doi.org/ 10.1016/j.carbpol. 2005.02.022.
31. Vanommeslaeghe, K.; Hatcher, E.; Acharya, C.; Kundu, S.; Zhong, S. *et. al.* CHARMM General Force Field: A force field for drug-like molecules compatible with the CHARMM all-atom additive biological force fields. *Journal of Computational Chemistry* **2010**, *31*, 671-690, https://doi.org/10.1002/jcc.21367.
32. Rissanou, A.N.; Harmandaris, V. A Molecular dynamics study of polymer/graphene nanocomposites. *Macromol. Symp* **2013**, *331-332*, 43-49, https://doi.org/10.1002/masy.201300070.
33. Martin, M.G.; Siepmann, J.I. Transferable potentials for phase equilibria. 1. United-atom description of *n*-alkanes. *J. Phys. Chem. B* **1998**, *102*, 2569-2577, https://doi.org/10.1021/jp972543+.
34. Walther, J.H.; Jaffe, R.; Halicioglu, T.; Koumoutsakos, P. Carbon nanotubes in water: Structural characteristics and energetics. *J. Phys. Chem. B* **2001**, *105*, 9980-9987, https://doi.org/10.1021/jp011344u.
35. Baschnagel, J. *et al.* Bridging the Gap Between Atomistic and Coarse-Grained Models of Polymers: Status and Perspectives. *In: Viscoelasticity, Atomistic Models, Statistical Chemistry. Advances in Polymer Science* **2000**, *152*, Springer, Berlin, Heidelberg, https://doi.org/10.1007/3-540-46778-5_2.
36. Deng, M.; Tan, V.B.C.; Tay, T.E. Atomistic modeling: interfacial diffusion and adhesion of polycarbonate and silanes. *Polymer* **2004**, *45*, 6399-6407, https://doi.org/10.1016/j.polymer.2004.06.055.
37. Fletcher, R. *Practical Methods of Optimization. Vol. 1, Unconstrained Optimization*. Horizon Pubs & Distributors Inc. **1980**, 1st edition.
38. Monajjemi, M. Cell membrane causes the lipid bilayers to behave as variable capacitors: A resonance with

self-induction of helical proteins. *Biophysical Chemistry* **2015**, *207*, 114-127, https://doi.org/10.1016/j.bpc.2015.10.003.
39. Monajjemi, M. Liquid-phase exfoliation (LPE) of graphite towards graphene: An ab initio study. *Journal of Molecular Liquids* **2017**, *230*, 461-472, https://doi.org/10.1016/j.molliq.2017.01.044.
40. Monajjemi, M.; Naderi, F.; Mollaamin, F.; Khaleghian, M. Drug design outlook by calculation of second virial coefficient as a nano study. *Journal of the Mexican Chemical Society* **2012**, *56*, 207-211, https://doi.org/10.29356/jmcs.v56i2.323.
41. Monajjemi, M. *et al*. Symmetry breaking of $B_2N^{(-,0,+)}$: An aspect of the electric potential and atomic charges. *Molecules* **2015**, *20*, 21636-21657, https://doi.org/10.3390/molecules201219769.
42. Monajjemi, M.; Mohammadian, N.T. S-NICS: An aromaticity criterion for nano molecules. *Journal of Computational and Theoretical Nanoscience* **2015**, *12*, 4895-4914, https://doi.org/10.1166/jctn.2015.4458.
43. Monajjemi, M.; Ketabi, S.; Hashemian Zadeh, M.; Amiri, A. Simulation of DNA bases in water: Comparison of the Monte Carlo algorithm with molecular mechanics force fields. *Biochemistry (Moscow)* **2006**, *71*, S1-S8, https://doi.org/10.1134/s0006297906130013.
44. Monajjemi, M.; Lee, V.S.; Khaleghian, M.; Honarparvar, B.; Mollaamin, F. Theoretical Description of Electromagnetic Nonbonded Interactions of Radical, Cationic, and Anionic $NH_2BHNBHNH_2$ Inside of the $B_{18}N_{18}$ Nanoring. *J. Phys. Chem C* **2010**, *114*, 15315-15330, https://doi.org/10.1021/jp104274z.
45. Monajjemi, M.; Boggs, J.E. A New Generation of B_nN_n Rings as a Supplement to Boron Nitride Tubes and Cages. *J. Phys. Chem. A* **2013**, *117*, 1670-1684, http://dx.doi.org/10.1021/jp312073q.
46. Monajjemi, M. Non bonded interaction between B_nN_n (stator) and $BN^{(-,0,+)}B$ (rotor) systems: A quantum rotation in IR region. *Chemical Physics* **2013**, *425*, 29-45, https://doi.org/10.1016/j.chemphys.2013.07.014.
47. Monajjemi, M.; Wayne Jr., R.; Boggs, J.E. NMR contour maps as a new parameter of carboxyl's OH groups in amino acids recognition: A reason of tRNA–amino acid conjugation. *Chemical Physics* **2014**, *433*, 1-11, https://doi.org/10.1016/j.chemphys.2014.01.017.
48. Monajjemi, M. Quantum investigation of non-bonded interaction between the $B_{15}N_{15}$ ring and BH_2NBH_2 (radical, cation, and anion) systems: a nano molecularmotor. *Struct Chem* **2012,** *23*, 551-580, http://dx.doi.org/10.1007/s11224-011-9895-8.
49. Monajjemi, M. Metal-doped graphene layers composed with boron nitride–graphene as an insulator: a nanocapacitor. *Journal of Molecular Modeling* **2014**, *20*, 2507, https://doi.org/10.1007/s00894-014-2507-y.
50. Monajjemi, M.; Heshmat, M.; Haeri, H.H.; Kaveh, F. Theoretical study of vitamin properties from combined QM-MM methods: Comparison of chemical shifts and energy. *Russian Journal of Physical Chemistry* **2006**, *80*, 1061-1068, https://doi.org/10.1134/S0036024406070119.
51. Monajjemi, M.; Honaparvar, B.; Khalili Hadad, B.; Ilkhani, A.; Mollaamin, F. Thermo-Chemical Investigation and NBO Analysis of Some anxileotic as Nano- Drugs. *African journal of pharmacy and pharmacology* **2010**, *4*, 521-529.
52. Monajjemi, M.; Najafpour, J.; Mollaamin, F. $(3,3)_4$ Armchair Carbon Nanotube in Connection with PNP and NPN Junctions: Ab Initio and DFT-Based Studies. *Fullerenes, Nanotubes and Carbon Nanostructures* **2013**, *21*, 213-232, https://doi.org/10.1080/1536383X.2011.597010.
53. Monajjemi, M.; Jafari Azan, M.; Mollaamin, F. Density Functional Theory Study on $B_{30}N_{20}$ Nanocage in Structural Properties and Thermochemical Outlook. *Fullerenes, Nanotubes and Carbon Nanostructures* **2013**, *21*, 503-515, https://doi.org/10.1080/1536383X.2011.629762.
54. Monajjemi, M.; Ghiasi, R.; Ketabi, S.; Passdar, H.; Mollaamin, F. A. Theoretical Study of Metal-Stabilised Rare Tautomers Stability: N4 Metalated Cytosine ($M=Be^{2+}$, Mg^{2+}, Ca^{2+}, Sr^{2+} and Ba^{2+}) in Gas Phase and Different Solvents. *Journal of Chemical Research* **2004**, *1*, 11-18, https://doi.org/10.3184/030823404323000648.
55. Monajjemi, M.; Baheri, H.; Mollaamin, F. A percolation model for carbon nanotube-polymer composites using the Mandelbrot-Given curve. *Journal of Structural Chemistry* **2011**, *52*, 54-59, https://doi.org/10.1134/S0022476611010070.
56. Mahlooji, E.; Atapour, M.; Labbaf, S. Electrophoretic deposition of Bioactive glass—Chitosan nanocomposite coatings on Ti-6Al-4V for orthopedic applications. *Carbohydr. Polym.* **2019**, *226*, 115299, https://doi.org/10.1016/j.carbpol.2019.115299.
57. Nie, L.; Wu, Q.; Long, H.; Hu, K.; Li, P.; Wang, C.; Sun, M.; Dong, J.; Wei, X.; Suo, J. *et al.* Development of chitosan/gelatin hydrogels incorporation of biphasic calcium phosphate nanoparticles for bone tissue engineering. *J. Biomater. Sci. Polym. Ed* **2019**, *30*, 1636-1657, https://doi.org/10.1080/09205063.2019.1654210.

58. Bartnikowski, M.; Dargaville, T.R.; Ivanovski, S.; Hutmacher, D.W. Degradation mechanisms of polycaprolactone in the context of chemistry, geometry and environment. *Prog. Polym. Sci.* **2019**, *96*, 1-20, https://doi.org/10.1016/j.progpolymsci.2019.05.004.
59. Neisiany, R.E.; Enayati, M.S.; Kazemi-Beydokhti, A.; Das, O.; Ramakrishna, S. Multilayered Bio-Based Electrospun Membranes: A Potential Porous Media for Filtration Applications. *Front. Mater.* **2020**, *7*, 67, https://doi.org/10.3389/fmats.2020.00067.
60. Khosravi, F.; Nouri Khorasani, S.; Rezvani Ghomi, E.; Kichi, M.K.; Zilouei, H.; Farhadian, M.; Esmaeely Neisiany, R. A bilayer GO/nanofibrous biocomposite coating to enhance 316L stainless steel corrosion performance. *Mater. Res. Exp.* **2019**, *6*, 086470, https://doi.org/10.1088/2053-1591/ab26d5.
61. Cobos, M.; De-La-Pinta, I.; Quindós, G.; Fernández, J.M.; Fernández, D.M. Synthesis, Physical, Mechanical and Antibacterial Properties of Nanocomposites Based on Poly(vinyl alcohol)/Graphene Oxide–Silver Nanoparticles. *Polymers* **2020**, *12*, 723, https://doi.org/10.3390/polym12030723.
62. Kouhi, M.; Jayarama Reddy, V.; Fathi, M.; Shamanian, M.; Valipouri, A.; Ramakrishna, S. Poly (3-hydroxybutyrate-co-3-hydroxyvalerate)/fibrinogen/bredigite nanofibrous membranes and their integration with osteoblasts for guided bone regenration. *J Biomed. Mater. Res.* **2019**, *107*, 1154-1165, https://doi.org/10.1002/jbm.a.36607.
63. Enayati, M.S.; Neisiany, R.E.; Sajkiewicz, P.; Behzad, T.; Denis, P.; Pierini, F. Effect of nanofiller incorporation on thermomechanical and toughness of poly (vinyl alcohol)-based electrospun nanofibrous bionanocomposites. *Theor. Appl. Fract. Mech.* **2019**, *99*, 44–50, https://doi.org/10.1016/j.tafmec.2018.11.006.
64. Fanaee, S.; Labbaf, S.; Enayati, M.H.; Baharlou Houreh, A.; Esfahani, M.-H.N. Creation of a unique architectural structure of bioactive glass sub-micron particles incorporated in a polycaprolactone/gelatin fibrous mat; characterization, bioactivity, and cellular evaluations. *J. Biomed. Mater. Res. Part A* **2019**, *107*, 1358-1365, https://doi.org/10.1002/jbm.a.36649.
65. Khalili, S.; Khorasani, S.N.; Neisiany, R.E.; Ramakrishna, S. Theoretical cross-link density of the nanofibrous scaffolds. *Mater. Des. Process. Commun.* **2019**, *1*, e22, https://doi.org/10.1002/mdp2.22.
66. Rezvani Ghomi, E.; Khalili, S.; Khorasani, S.N.; Neisiany, R.E.; Ramakrishna, S. Wound dressings: Current advances and future directions. *J. Appl. Polym. Sci.* **2019**, *136*, 47738, https://doi.org/10.1002/app.47738.
67. Neisiany, R.E.; Enayati, M.S.; Sajkiewicz, P.; Pahlevanneshan, Z.; Ramakrishna, S. Insight into the Current Directions in Functionalized Nanocomposite Hydrogels. *Front. Mater.* **2020**, *7*, 25, https://doi.org/10.3389/fmats.2020.00025.
68. Bemenderfer, T.B.; Davis, W.H.; Anderson, R.B.; Wing, K.; Escudero, M.I.; Waly, F.; Penner, M. Heterotopic ossification in total ankle arthroplasty: Case series and systematic review. *J. Foot Ankle Surg.* **2020**, *59*, 716-721, https://doi.org/10.1053/j.jfas.2019.12.003.
69. Tabesh, E.; Salimijazi, H.; Kharaziha, M.; Mahmoudi, M.; Hejazi, M. Development of an in-situ chitosan-copper nanoparticle coating by electrophoretic deposition. *Surf. Coat. Technol.* **2019**, *364*, 239-247, https://doi.org/10.1016/j.surfcoat.2019.02.040.
70. Tabesh, E.; Kharaziha, M.; Mahmoudi, M.; Shahnam, E.; Rozbahani, M. Biological and corrosion evaluation of Laponite: Poly(caprolactone) nanocomposite coating for biomedical applications. *Colloids Surf. A: Physicochem. Eng. Asp.* **2019**, *583*, 123945, https://doi.org/10.1016/j.colsurfa.2019.123945.
71. Mahmoudi, M.; Raeissi, K.; Karimzadeh, F.; Golozar, M. A study on corrosion behavior of graphene oxide coating produced on stainless steel by electrophoretic deposition. *Surf. Coat. Technol.* **2019**, *372*, 327-342, https://doi.org/10.1016/j.surfcoat.2019.05.050.
72. Kichi, M.K.; Torkaman, R.; Mohammadi, H.; Toutounchi, A.; Kharaziha, M.; Alihosseini, F. Electrochemical and *in vitro* bioactivity behavior of Poly (ε-caprolactone)(PCL)-Gelatin-Forsterite Nano Coating on Titanium for Biomedical Application. *Mater. Today Commun.* **2020**, *24*, 101326, https://doi.org/10.1016/j.mtcomm.2020.101326.
73. Mesquita-Guimarães, J.; Ramos, L.; Detsch, R.; Henriques, B.; Fredel, M.; Silva, F.; Boccaccini, A.R. Evaluation of *in vitro* properties of 3D micro-macro porous zirconia scaffolds coated with 58S bioactive glass using MG-63 osteoblast-like cells. *J. Eur. Ceram. Soc.* **2019**, *39*, 2545-2558, https://doi.org/10.1016/j.jeurceramsoc.2019.01.029.
74. Boodagh, P.; Johnson, R.; Maly, C.; Ding, Y.; Tan, W. Soft-sheath, stiff-core microfiber hydrogel for coating vascular implants. *Colloids Surf. B: Biointerfaces* **2019**, *183*, 110395, https://doi.org/10.1016/j.colsurfb.2019.110395.
75. Khosravi, F.; Khorasani, S.N.; Khalili, S.; Neisiany, R.E.; Ghomi, E.R.; Ejeian, F.; Das, O.; Nasr-Esfahani,

M.H. Development of a Highly Proliferated Bilayer Coating on 316L Stainless Steel Implants. *Polymers* **2020**, *12*, 1022, https://doi.org/10.3390/polym12051022.
76. Govindan, R.; Gu, F.; Karthi, S.; Girija, E. Effect of phosphate glass reinforcement on the mechanical and biological properties of freeze-dried gelatin composite scaffolds for bone tissue engineering applications. *Mater. Today Commun.* **2020**, *22*, 100765, https://doi.org/10.1016/j.mtcomm.2019.100765.
77. Pokorski, J.K.; Hore, M.J. Structural characterization of protein–polymer conjugates for biomedical applications with small-angle scattering. *Curr. Opin. Colloid Interface Sci.* **2019**, *42*, 157-168, https://doi.org/10.1016/j.cocis.2019.08.001.
78. Alizadeh-Osgouei, M.; Li, Y.; Wen, C. A comprehensive review of biodegradable synthetic polymer-ceramic composites and their manufacture for biomedical applications. *Bioact. Mater.* **2019**, *4*, 22-36, https://doi.org/10.1016/j.bioactmat.2018.11.003.
79. Zahran, M.; Marei, A.H. Innovative natural polymer metal nanocomposites and their antimicrobial activity. *Int. J. Biol. Macromol.* **2019**, *136*, 586-596, https://doi.org/10.1016/j.ijbiomac.2019.06.114.
80. Abrisham, M. *et al.* The Role of Polycaprolactone-Triol (PCL-T) in Biomedical Applications: A state-of-the-art review. *Eur. Polym. J.* **2020**, *131*, 109701, https://doi.org/10.1016/j.eurpolymj.2020.109701.
81. Jia, L.; Han, F.; Wang, H.; Zhu, C.; Guo, Q.; Li, J.; Zhao, Z.; Zhang, Q.; Zhu, X.; Li, B. Polydopamine-assisted surface modification for orthopaedic implants. *J. Orthop. Transl.* **2019**, *17*, 82-95, https://doi.org/10.1016/j.jot.2019.04.001.
82. Avcu, E.; Bastan, F.E.; Abdullah, H.Z.; Rehman, M.A.U.; Avcu, Y.Y.; Boccaccini, A.R. Electrophoretic deposition of chitosan-based composite coatings for biomedical applications: A review. *Prog. Mater. Sci.* **2019**, *103*, 69-108, https://doi.org/10.1016/j.pmatsci.2019.01.001.
83. Gadkari, S.; Gu, S.; Sadhukhan, J. Two-dimensional mathematical model of an air-cathode microbial fuel cell with graphite fiber brush anode. *J. Power Sources* **2019**, *441*, 227145, https://doi.org/10.1016/j.jpowsour.2019.227145.
84. Kocijan, A.; Conradi, M.; Hocevar, M. The influence of surface wettability and topography on the bioactivity of TiO_2/epoxy coatings on AISI 316L stainless steel. *Materials* **2019**, *12*, 1877, https://doi.org/10.3390/ma12111877.